Diminished Immune Surveillance during Histologic Progression of Intraductal Papillary Mucinous Neoplasms Offers a Therapeutic Opportunity for Cancer Interception

Sharia Hernandez[1], Edwin Roger Parra[1], Naohiro Uraoka[1], Ximing Tang[1], Yu Shen[2], Wei Qiao[2], Mei Jiang[1], Shanyu Zhang[1], Barbara Mino[1], Wei Lu[1], Renganayaki Pandurengan[1], Cara Haymaker[1], Kajsa Affolter[3], Courtney L. Scaife[4], Michele Yip-Schneider[5], C. Max Schmidt[5], Matthew A. Firpo[4], Sean J. Mulvihill[4], Eugene J. Koay[6], Huamin Wang[7], Ignacio I. Wistuba[1], Anirban Maitra[1,7], Luisa M. Solis[1], and Subrata Sen[1]

ABSTRACT

Purpose: Intraductal papillary mucinous neoplasms (IPMN) are bona fide precursors to pancreatic ductal adenocarcinoma (PDAC). While genomic alterations during multistep IPMN progression have been well cataloged, the accompanying changes within the tumor immune microenvironment (TIME) have not been comprehensively studied. Herein, we investigated TIME-related alterations during IPMN progression, using multiplex immunofluorescence (mIF) coupled with high-resolution image analyses.

Experimental Design: Two sets of formalin-fixed, paraffin-embedded tissue samples from surgically resected IPMNs were analyzed. The training set of 30 samples consisted of 11 low-grade IPMN (LG-IPMN), 17 high-grade IPMN (HG-IPMN), and 2 IPMN with PDAC, while a validation set of 93 samples comprised of 55 LG-IPMN and 38 HG-IPMN. The training set was analyzed with two panels of immuno-oncology–related biomarkers, while the validation set was analyzed with a subset of markers found significantly altered in the training set.

Results: Cell types indicative of enhanced immune surveillance, including cytotoxic and memory T cells, and antigen-experienced T cells and B cells, were all found at higher densities within isolated LG-IPMNs compared with HG-IPMNs. Notably, the TIME of LG-IPMNs that had progressed at the time of surgical resection (progressor LGD) resembled that of the synchronous HG-IPMNs, underscoring that attenuated immune surveillance occurs even in LG-IPMNs destined for progression.

Conclusions: Our findings provide a basis for interception of cystic neoplasia to PDAC, through maintenance of sustained immune surveillance using vaccines and other prevention approaches.

Introduction

Intraductal papillary mucinous neoplasms (IPMN) of the pancreas are mucin-secreting, cystic precursor lesions of pancreatic ductal adenocarcinoma (PDAC; ref. 1). Histologically they are either isolated or multicentric cysts of more than 5 mm, arising within the main or branch pancreatic duct, with papillary structures lined by mucinous columnar epithelium and varying grades of cellular atypia (2). IPMNs involving the main duct and mixed main-branch duct have higher risk of progressing to invasive cancer than those confined to the branch ducts (3, 4). These cystic lesions are graded using a two-tier system based on the degree of dysplasia observed: low-grade IPMN (LG-IPMN), characterized by mild to moderate grade of epithelial dysplasia, and high-grade IPMN (HG-IPMN), characterized by high-grade epithelial dysplasia, previously known as carcinoma *in situ* (5). Patients with noninvasive IPMNs have excellent prognosis upon surgical resection, but once an IPMN develops an invasive component, the probability of long-term survival drops significantly (6). In addition, it is estimated that approximately 2% of IPMN cases that are surgically resected will develop an invasive PDAC in the remnant pancreas (7). Next-generation sequencing studies have shown that IPMNs share several genetic alterations with PDAC, such as presence of mutant *KRAS, GNAS, TP53, SMAD4 PTEN*, and *PIK3CA*, among others (8–10). In contrast to melanoma or lung cancers, PDAC is predominantly an immunologically "cold" malignancy, which is largely recalcitrant to immunotherapy (11, 12). Immune profiling studies of the PDAC tumor immune microenvironment (TIME) has revealed a complex network of immune suppressive cellular and cytokine interactions, resulting in minimal treatment benefit from immune checkpoint–blocking agents (13). In addition, PDAC tumor subtypes with distinct immune infiltration phenotypes have been recognized as "immune rich," "immune escape," and "immune exhausted" (14–17). While "immune rich" were reported to have high abundance of T and B cells along with low $FOXP3^+$ regulatory T cells (Treg), "immune escape" subtypes were characterized by opposite immune profiles and the "immune exhausted" with immunogenic microenvironment containing subpopulations of PD-L1–expressing

[1]Department of Translational Molecular Pathology, University of Texas MD Anderson Cancer Center, Houston, Texas. [2]Department of Biostatistics, University of Texas MD Anderson Cancer Center, Houston, Texas. [3]Department of Pathology, University of Utah, Salt Lake City, Utah. [4]Department of Surgery, University of Utah, Salt Lake City, Utah. [5]Department of Surgery, Indiana University School of Medicine, Indianapolis, Indiana. [6]Department of Radiation Oncology, University of Texas MD Anderson Cancer Center, Houston, Texas. [7]Department of Pathology, University of Texas MD Anderson Cancer Center, Houston, Texas.

Note: Supplementary data for this article are available at Clinical Cancer Research Online (http://clincancerres.aacrjournals.org/).

S. Hernandez, E.R. Parra, L.M. Solis, and S. Sen contributed equally to this article.

Corresponding Authors: Subrata Sen, PhD, University of Texas MD Anderson Cancer Center, Department of Translational Molecular Pathology, 2130 West Holcombe Boulevard, Houston, TX 77030. E-mail: ssen@mdanderson.org; and Luisa M. Solis, MD, lmsolis@mdanderson.org

Clin Cancer Res 2022;28:1938–47

doi: 10.1158/1078-0432.CCR-21-2585

Translational Relevance

Intraductal papillary mucinous neoplasms (IPMN) are well-recognized cystic precursor lesions of pancreatic ductal adenocarcinoma. Current standard-of-care guidelines for patients with pancreatic cyst recommend either surgical excision of the lesions or longitudinal passive surveillance using radiology and cyst fluid biomarkers. In this study, we interrogated alterations within the tumor immune microenvironment (TIME) of IPMNs of varying histologic grades. Our findings demonstrate that diminished immune surveillance is a feature of high-grade IPMNs (HG-IPMN), and that such attenuation is also seen within the TIME of "progressor" low-grade IPMNs (IPMN) present within the vicinity of synchronous HG-IPMN. These findings provide a basis for initiating interception trials using vaccines or immune checkpoint inhibitors that can enhance or sustain immune surveillance within TIME of IPMN, and potentially block progression to invasive neoplasia.

cells displaying microsatellite instability. Interestingly, PDACs arising from IPMN have been associated with classical (pancreatic progenitor) subtype and prevalent microsatellite instability harboring immunogenic microenvironment but immune-exhausted phenotype (15, 18) In contrast, squamous PDAC subtype (alias "quasi-mesenchimal" or "basal-like") was reported to display an immune escape phenotype (15, 16). In view of these observations, it is important that the immune microenvironment of precursor lesions, such as IPMNs, is characterized in detail to elucidate the role of innate and adaptive immunity during the multistep progression of PDAC. Previously, limited analyses of the TIME of IPMN has demonstrated that HG-IPMNs have higher numbers of myeloid-derived suppressor cells (MDSC) and Tregs, compared with normal ductal epithelium or LG-IPMNs, suggesting immune suppressive mechanisms come into effect with progression of the disease (19). Similarly, a recent study analyzing spatial distribution of T-cell subsets in IPMN progression reported that the immune microenvironment evolves from a diverse T-cell mixture in LG-IPMNs to a Treg-dominated immunosuppressive state in invasive PDAC (20). However, an in depth, high-dimensional analysis of the TIME of IPMNs, including independent assessment of LG-IPMNs that are isolated *versus* ones that have synchronously progressed to HG-IPMN or PDAC has not been conducted. Such an analysis could provide unprecedented insights into whether IPMNs that are destined to progress in their natural history demonstrate immunologic alterations in the TIME even at the stage of LG dysplasia (LGD), thereby opening a potential window of opportunity for immune interception.

One of the more informative approaches to study the immune microenvironment of these heterogeneous lesions is the use of multiplex IHC and immunofluorescence assays, which allow for the assessment of multiple biomarkers using a single-tissue section, and their coexpression in different immune cell types (21, 22). Application of this analytic approach in IPMN can also reveal the spatial relationships of the immune infiltrate within the dysplastic epithelium and proximal stroma at different stages of preneoplasia. In the current study, we investigated the landscape of TIME in a large series of IPMNs of all histologic grades of epithelial dysplasia, using selected immuno-oncology biomarkers of adaptive and innate immune response by IHC and multiplex immunofluorescence (mIF). The rigor of our analysis was underscored by using training and validation sets of cases. In addition to immune cell subtyping, we also addressed the question of divergence in TIME between LGD from LG-IPMN (*isolated LGD*) and LGD from HG-IPMN (*progressor LGD*). To the best of our knowledge, our dataset is the most extensive assessment of the TIME of IPMN and will form the foundational basis for implementing interception efforts in this PDAC precursor.

Materials and Methods

Patients and samples

A training set of 30 formalin-fixed paraffin-embedded (FFPE) IPMN tissue samples from The University of Texas MD Anderson Cancer (Houston, TX) and a second validation set of 93 FFPE-IPMN samples from the University of Utah Huntsman Cancer Institute (Salt Lake City, Utah) and Indiana University School of Medicine (Indianapolis, IN) were analyzed in this study. All tissue samples were from patients who underwent surgical treatment without neoadjuvant therapy at these institutions and the study was performed under approved protocols of the respective Institutional Review Boards (IRB) according to the principles of the Helsinki Declaration (23). All patients provided written informed consent for this IRB protocol. For the training set, clinicopathologic information, including sex, age, race, smoking status, alcohol use, diabetes history, and pathologic characteristics (tumor location, cyst size, and histologic grade) was available for all cases (Supplementary Table S1).

The diagnostic slides were histologically reviewed by two expert pancreatic cancer pathologists (H. Wang and A. Maitra). Each case was classified following the international consensus Fukuoka guidelines (1). The training set comprised of 11 LG-IPMN (presence of only low- to intermediate-grade dysplasia), 17 HG-IPMN [presence of high-grade dysplasia (HGD)], and 2 IPMN with invasive adenocarcinoma, while the validation set had 55 LG-IPMN and 38 HG-IPMN, based on the highest degree of epithelial dysplasia in diagnostic hematoxylin and eosin (H&E) slides. Of note, for the purpose of analysis, we classified the LGD areas as "isolated LGD," when there was no HGD in an IPMN, and "progressor LGD" when an IPMN contained synchronous LGD and HGD. Detailed information of histologic subtype (gastric/intestinal/pancreatobiliary) from the cases from the training set is presented in Supplementary Table S2. From each sample, we selected FFPE tissue block containing the highest grade of dysplasia, and representative areas of all grade of dysplasia within the lesion. Blocks were cut in consecutives serial sections of 4 μm thickness. Slides were stained with the two mIF panels and conventional single IHC for CD20 (B cells), the latter as validation for the CD20 marker included in one of the mIF panels, and to explore the lymphoid aggregates associated with IPMN.

Identification of regions of interest for digital image analysis

Regions of interest (ROI) in the H&E-stained tissue sections, representing distinct histopathologic features, were selected for conventional IHC and mIF analyses. The H&E samples were scanned at 20×, using Aperio AT2 scanner (Leica Biosystem) and the images were visualized with Aperio ImageScope (Leica Biosystem) software. LGD, HGD, and invasive PDAC were identified and annotated. We selected regions of interest (ROI) for the following types of lesions: (i) LGD areas of LG-IPMN (isolated LGD), (ii) LGD areas of HG-IPMN (progressor LGD), (iii) HGD areas of HG-IPMN, and (iv) additional areas with invasive adenocarcinoma for IPMN with PDAC (detailed information on the number of ROIs analyzed in each category are

Table 1. Immunophenotyping by mIF using two OPAL panels.

Phenotype	Biomarker expression
Opal Panel 1	
Epithelial cells	$(CK^+PD\text{-}L1^+) + (CK^+)$
Epithelial cells PD-L1$^+$	$CK^+PD\text{-}L1^+$
Total T-cell lymphocytes	$(CD3^+ \text{ only}) + (CD3^+CD8^+PD1^-) + (CD3^+PD1^+) + (CD3^+CD8^+PD1^+)$
Cytotoxic T cells	$(CD3^+CD8^+PD1^-) + (CD3^+CD8^+PD1^+)$
T cells, antigen experienced	$(CD3^+PD1^+) + (CD3^+CD8^+PD1^+)$
Total macrophages	$(CD68^+PD\text{-}L1^-) + (CD68^+PD\text{-}L1^+)$
Macrophages PD-L1$^+$	$CD68^+PD\text{-}L1^+$
Opal Panel 2	
Total B-cell lymphocytes	$CD20^+$
CD45RO$^+$ cells	$CD45RO^+$
Granzyme B$^+$ cells	Granzyme B^+
FOXP3$^+$ cells	$FOXP3^+$
CD57$^+$ cells	$CD57^+$

shown in Supplementary Table S3). Areas beyond the fibrous band, areas with chronic pancreatitis, and cyst rupture were not included in the ROIs. Minimum and maximum distances among progressor LGD and HGD areas of HG-IPMN are shown in Supplementary Table S4.

mIF and digital image analysis

Marker panels for mIF were used to characterize the immune microenvironment in the ROIs of IPMN lesions in LGD, HGD, and PDAC (**Table 1**). Staining and processing methodology was described previously (21, 22) including the antibodies described in Supplementary Table S5. The slides were scanned at low resolution (10×) using a multispectral microscope (Vectra 3.0 system, Akoya biosciences). Pathologists performing the analyses (N. Uraoka, E.R. Parra, S. Hernandez, and X. Tang) selected the ROIs (660 μm × 500 μm, 0.33 mm^2 each), guided by the H&E-stained histopathologic features following review by the two expert pancreatic cancer pathologists (H. Wang and A. Maitra), mentioned above. The ROIs were scanned at 20× resolution for digital imaging analysis using the InForm 2.0.4 software (Akoya Biosciences; **Fig. 1**). Each ROI was classified into two compartments: the dysplastic epithelial/carcinoma compartment (EC), defined as an area having dysplastic epithelium or invasive carcinoma cells including immune cells in between the dysplastic epithelial cells or the stroma in contact with the basal membrane, and the stromal compartment (ST) represented by the stroma tissue that is adjacent to the dysplastic epithelial/carcinoma compartment including immune cells that are not in contact with the basal membrane (Supplementary Fig. S1). Distribution of area sizes in mm^2 for dysplastic epithelial/carcinoma, stromal, and total compartments of the training set and the validation set are provided in Supplementary Table S6. The following markers were evaluated in panel 1: PD-L1,

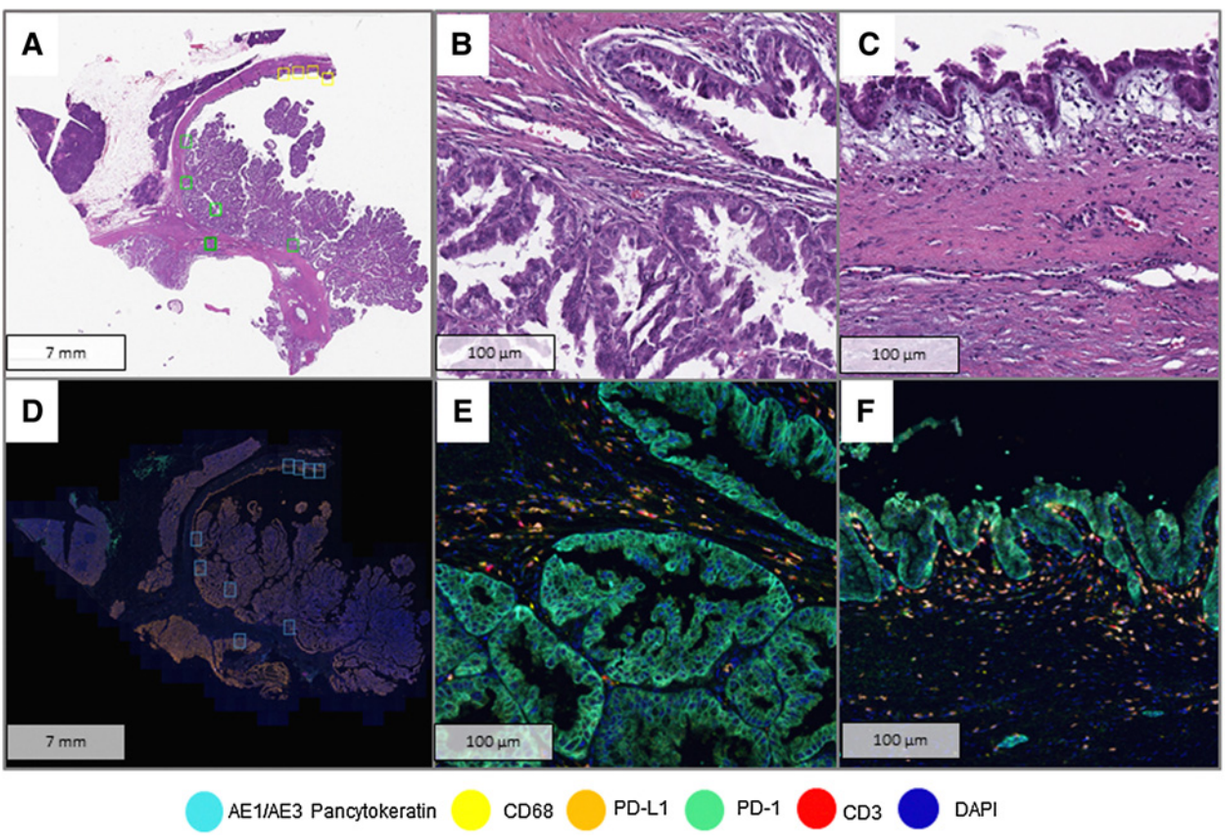

Figure 1.
Analysis of immune cell infiltrates using mIF. **A,** Whole-section H&E slide of a high-grade IPMN with HGD areas (yellow squares) and LGD areas (green squares) selected for digital image analysis. **B,** HGD area at high resolution (40×). **C.** LGD area at high resolution (40×). **D,** Image scan of Phenochart with selected areas for high magnification (blue squares). **E,** Panel 1 composite of HGD area (40×). **F,** Panel 1 composite of LGD area.

PD1, CD3, CD8, CD68, CK (AE1/AE3), and DAPI, while the second panel included the following markers: CD20, CD45RO, CD57, granzyme B, FOXP3, CK (AE1/AE3), and DAPI (Supplementary Table S7). Cells coexpressing the markers (representing the cell phenotypes) including epithelial/malignant cells [CK^+; cytokeratin marker, epithelial/malignant cells expressing PD-L1 ($CK^+PD\text{-}L1^+$)]; T lymphocytes [$CD3^+$; pan T-cell marker, including cytotoxic T cells ($CD3^+CD8^+$), antigen-experienced T cells ($CD3^+PD\text{-}1^+$), cytotoxic antigen-experienced T cells ($CD3^+CD8^+PD\text{-}1^+$); tumor-associated macrophages [TAM ($CD68^+$)]; and TAMs expressing PD-L1 ($CD68^+$ $PD\text{-}L1^+$) were well characterized in panel 1 while individual markers were analyzed as part of the panel 2 (**Table 1**). The final results were expressed as the number of cells/mm^2 from different cell populations. For PD-L1, a cutoff >1% membranous expression of epithelial or malignant cells was considered as positive for statistical analysis.

Evaluation of B-cell lymphoid aggregates by conventional single-marker IHC

In parallel, sequential tissue sections (4 μm thickness) were stained in a Leica Bond Max automated stainer (Leica Biosystems) for CD20 IHC to examine possible induction of B-cell lymphoid aggregates in the training cohort. The tissue sections were deparaffinized and rehydrated following the Leica Bond protocol. Antigen retrieval was performed for 20 minutes with Bond Solution #2 (Leica Biosystems, equivalent EDTA, pH 9.0). The primary antibody (CD20, clone L-26, Agilent Dako, catalog no. M0755, dilution 1:1,400), was incubated for 15 minutes at room temperature and detected using the Bond Polymer Refine Detection kit (Leica Biosystems) with 3,3′-diaminobenzidine (DAB) as chromogen. The slides were counterstained with hematoxylin. The IHC-stained slides were scanned with Aperio AT2 scanner (Leica Biosystem) at 20× magnification; the images were visualized and analyzed with Halo (Indica Lab) image analysis software. Presence of B-cell lymphoid aggregates, defined as organized groups of $CD20^+$ cells (24), was annotated by pathologists (S. Hernandez, L.M. Solis) in the tissue surrounding the cyst (excluding cyst content). Then, we quantified their number, extension area (mm^2), and the nearest distance (μm^2) of the lymphoid aggregates to the dysplastic epithelium. In parallel, for internal validation of the mIF data, we quantified $CD20^+$ cell densities obtained by IHC; similar to the ROI selection strategy used for mIF, CD20-positive cells were quantified in the dysplastic epithelial/carcinoma and stromal compartments of each ROI placed in the areas used for mIF. We used the "cytonuclear v1.6" algorithm (Halo, IndicaLab) and the results were reported as cell densities (n/mm^2) from the total areas of each compartment analyzed (**Fig. 2**).

Statistical analysis

Statistical analysis was mainly descriptive. χ^2 or Fisher exact test were used to evaluate associations between categorical clinicopathologic variables and histologic classifications of IPMNs. To determine associations of clinicopathologic variables and cell densities of each cell type of HG-IPMN and LG-IPMN, we used the *t* test, using the average cell density of LGD and HGD areas for each IPMN case per each compartment (EC, ST, and EC+ST). To test differences between cell densities of paired progressor LGD and HGD areas from HG-IPMN, we used the Wilcoxon signed-rank test. To test differences between isolated LGD, progressor LGD, and HGD areas, we applied Kruskal–Wallis; to test differences between the two groups, we used *t* test.

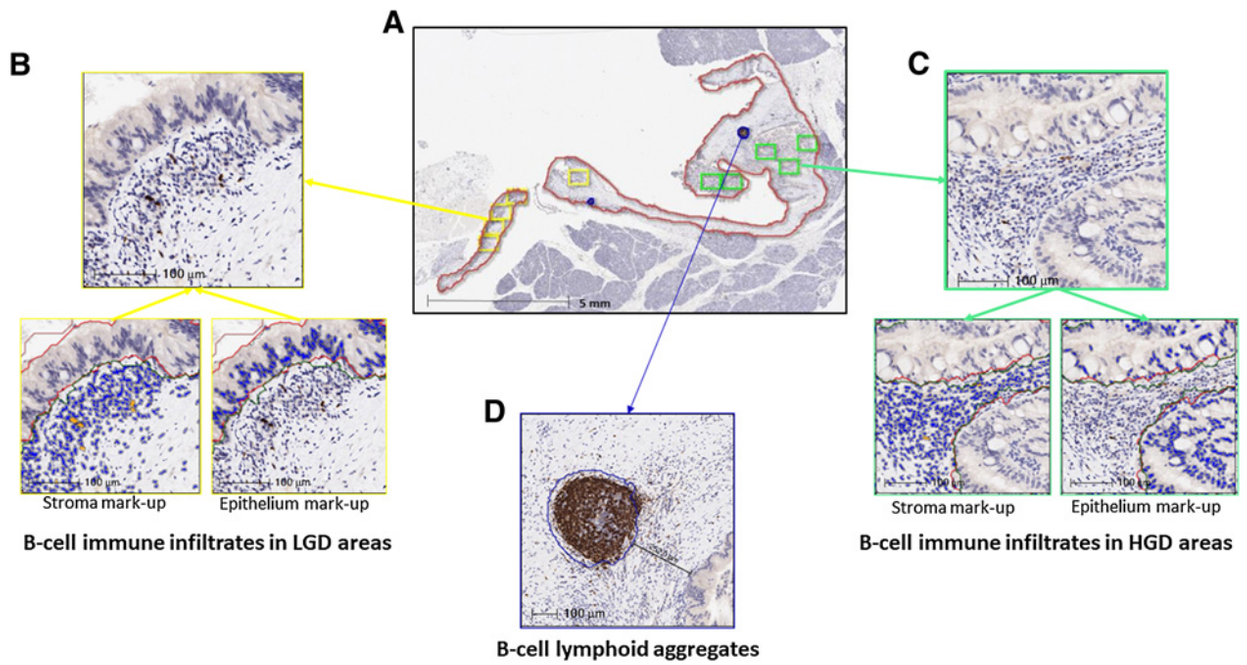

Figure 2.
Analysis of B-cell immune infiltrates and B-cell lymphoid aggregates in IPMNs by IHC for CD20 and digital image analysis. **A,** Low-magnification image of a high-grade IPMN with cyst area (red line), B-cell lymphoid aggregates (blue line), LGD (yellow boxes), and HGD (green boxes) areas selected for image analysis. **B** and **C** show high-magnification images of LGD and HGD areas and mark-up images of CD20-positive cells (orange) in stromal and dysplastic epithelial compartments. **D** shows a high-magnification image of a B-cell lymphoid aggregate (blue line).

Spearman correlation estimation and test for a rank-based measure of association was also applied. Statistical analysis was carried out using SAS version 9.4 (SAS Institute) or GraphPad software. $P < 0.05$ was considered statistically significant. Wilcoxon rank-sum test was used to assess the difference of the immune cell densities in the epithelial compartment of HG-IPMN in the following ways: (i) regardless of the grade of dysplasia, (ii) between "closest" and "furthest" HGD areas to the progressor LGD, and (iii) between "closest" and "furthest" progressor LGD areas to HGD (Supplementary Table S8A–S8C).

Data availability

The data generated in this study are available upon request from the corresponding authors.

Results

Immune profiling of LG and HG-IPMN using a training set

Using a training set, we first evaluated biomarkers to address the PD-L1/PD1 axis and relevant tumor-associated immune cells in the TIME of LG- and HG-IPMNs. The clinicopathologic characteristics of the samples from this set are described in Supplementary Table S1. Associations of immune cell densities with clinicopathologic features in different compartments are shown in Supplementary Table S7 and Supplementary Fig. S2. Interestingly, in the epithelial compartment, the densities of T cells, cytotoxic T cells, and granzyme B cells were significantly higher in gastric subtype compared with intestinal or pancreatobiliary, and most IPMN of gastric subtypes were LG-IPMN (10/17, 59%; Supplementary Table S9). In this training cohort, no associations were observed between histologic classifications of IPMN (LG-IPMN and HG-IPMN) and clinicopathologic characteristics.

The mIF analysis of dysplastic epithelial cells showed PD-L1–positive expression in three HG-IPMNs, though in all of them expression was heterogeneous. Two of them exhibited PD-L1 in 39.7% and 1.7% of the epithelial cells of HGD areas, while no PD-L1 expression was observed in progressor LGD; one IPMN exhibited PD-L1 expression in 19.5% of the epithelial cells in progressor LGD while no expression was observed in the HGD epithelium. Evaluation of the immune cells by mIF showed higher densities of

Table 2. Analysis of immune biomarkers in LGD and HGD areas of Intraductal papillary mucinous neoplasm in the training set.

	Isolated LGD areas of LG-IPMN		Progressive LGD areas of HG-IPMN		HGD areas of HG-IPMN		
Phenotype	**Median**	**SD**	**Median**	**SD**	**Median**	**SD**	***P*[a]**
Dysplastic epithelial compartment							
$CD3^+$ (n/mm^2)	329	210	99	211	140	120	0.017
$CD3^+CD8^+$ (n/mm^2)	38	86	9	104	13	53	0.047
$CD3^+PD1^+$ (n/mm^2)	0	4	0	9	0	2	0.800
$CD68^+$ (n/mm^2)	10	35	22	34	12	29	0.910
$CD68^+$PD-$L1^+$ (%)	22	30	27	33	25	20	0.658
$CD20^+$ (n/mm^2)	2	4	0	3	0	4	0.030
$CD45RO^+$ (n/mm^2)	188	83	62	79	63	81	0.008
$CD57^+$ (n/mm^2)	23	63	40	88	17	47	0.734
Granzyme B^+ (n/mm^2)	95	42	34	74	37	61	0.022
$FOXP3^+$ (n/mm^2)	2	2	1	7	0	6	0.580
Stromal compartment							
$CD3^+$ (n/mm^2)	588	676	684	650	659	891	0.971
$CD3^+CD8^+$ (n/mm^2)	210	321	194	246	130	185	0.610
$CD3^+PD1^+$ (n/mm^2)	7	45	4	64	9	27	0.521
$CD68^+$ (n/mm^2)	97	114	204	252	210	169	0.296
$CD68^+$PD-$L1^+$ (%)	28	24	32	24	36	18	0.998
$CD20^+$ (n/mm^2)	23	299	14	38	7	87	0.579
$CD45RO^+$ (n/mm^2)	784	536	607	520	547	585	0.659
$CD57^+$ (n/mm^2)	76	208	89	105	78	75	0.931
Granzyme B^+ (n/mm^2)	348	473	320	333	241	288	0.816
$FOXP3^+$ (n/mm^2)	24	24	12	75	19	31	0.733
Dysplastic epithelial and stroma compartment							
$CD3^+$ (n/mm^2)	521	487	474	447	470	308	0.724
$CD3^+CD8^+$ (n/mm^2)	172	234	133	197	63	138	0.545
$CD3^+PD1^+$ (n/mm^2)	4	31	2	18	7	12	0.372
$CD68^+$ (n/mm^2)	64	69	91	98	146	108	0.300
$CD68^+$PD-$L1^+$ (%)	28	23	31	25	36	18	0.999
$CD20^+$ (n/mm^2)	14	149	9	26	5	20	0.370
$CD45RO^+$ (n/mm^2)	495	324	321	372	347	301	0.277
$CD57^+$ (n/mm^2)	63	113	82	101	47	62	0.926
Granzyme B^+ (n/mm^2)	250	287	190	238	167	188	0.576
$FOXP3^+$ (n/mm^2)	15	14	7	48	10	16	0.787

Abbreviations: HGD, high-grade dysplasia; HG-IPMN, high-grade intraductal papillary mucinous neoplasm; LG-IPMN, low-grade intraductal papillary mucinous neoplasm; LGD, low-grade dysplasia.
[a]Kruskal–Wallis.

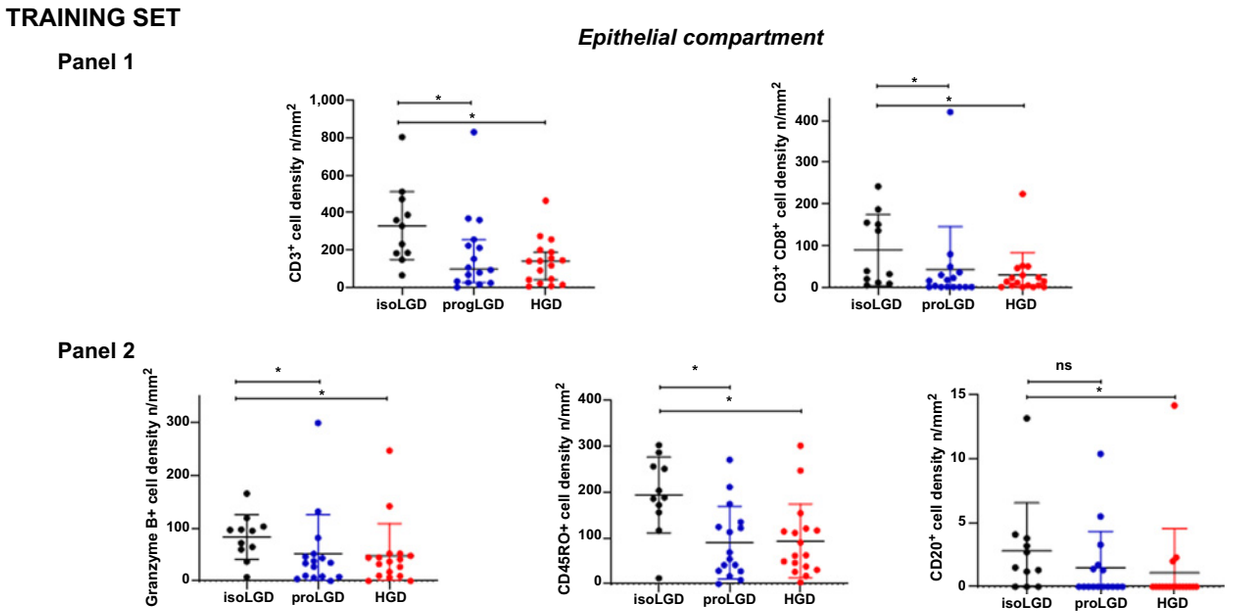

Figure 3.

Scatter dot plot showing differential distribution of immune cell densities in the dysplastic epithelial compartment of the Training set, among dysplasia areas of low-grade IPMN and high-grade IPMN (isoLGD, isolated low-grade dysplasia area of low-grade IPMN; progLGD, progressive low-grade dysplasia area of high-grade IPMN; HGD, high-grade dysplasia area of high-grade IPMN). Panel 1: $CD3^+$, $CD3^+CD8^+$; Panel 2: Granzyme B+, CD45RO+, and CD20+. Differences between all groups were determined using Kruskal–Wallis, and differences between two groups were determined by *t* test (ns, nonsignificant). Black bars indicate median and 95% confidence Interval.

overall T cells, cytotoxic T cells, $CD45RO^+$, and granzyme B+ cells in the dysplastic epithelial compartment of LG-IPMN compared with HG-IPMN (**Table 2**). Further analysis based on the degree of dysplasia of IPMN showed higher densities of the same cell types in the epithelial/proximal stromal compartment of isolated LGD of LG-IPMNs compared with progressor LGD of HG-IPMN, as well as HGD areas of HG-IPMN (**Fig. 3**). No differences of antigen-experienced T cells, macrophages, PD-$L1^+$, $CD57^+$, or $FOXP3^+$ cells were found in this compartment (Supplementary Fig. S3). We did not find differences among LG-IPMN and HG-IPMN when comparing the cell densities in the stromal compartment (Supplementary Fig. S4). Paired analysis of progressor LGD and HGD areas of HG-IPMNs ($n = 16$) showed that $CD20^+$ cell densities were higher in the dysplastic epithelial compartment of progressor LGD ($P = 0.031$; Supplementary Fig. S5). The two IPMN cases with invasive adenocarcinoma showed heterogenous distribution of immune infiltrates (Supplementary Table S10).

To assess how the distance may impact the associations found between progressor LGD and HGD in the epithelial compartment, we compared the cell densities of the immunophenotypes of the epithelial compartment of progressor LGD ROIs that were "closest" to HGD ROI with the ones that were "furthest" away from a HGD ROI; similar comparison was performed using HGD ROIs that were closest and furthest away from the LGD ROIs. On the basis of the comparison, focusing on the epithelial compartment, no statistically significant difference in immune cell densities was detected between the LGD and HGD ROIs at varying distances in any of the groups (Supplementary Table S8A–S8C).

Then we evaluated the presence of B cells using single chromogenic IHC for CD20 to determine and quantify the presence of B-cell lymphoid aggregates and $CD20^+$ cell densities. B-cell lymphoid aggregates were found in 19 IPMN (68%) cases (12 HG-IPMN and 7 LG-IPMN). The number of lymphoid aggregates per mm^2 and their area extension per mm^2 showed no significant associations between LG-IPMN compared with HG-IPMN (Supplementary Table S11), and none of these aggregates had noticeable germinal centers. We believe presence of lymphoid aggregates should be investigated in a larger cohort. For internal validation, comparison of $CD20^+$ cell densities with the results of mIF revealed moderate (EC) or high (ST and EC+ST) correlation with the corresponding results of mIF in all compartments analyzed (EC: Spearman rho = 0.36, $P = 0.019$; ST: rho = 0.77, $P < 0.0001$; E+ST: rho = 0.71, $P < 0.0001$). We did not find statistically significant difference when comparing LGD with HGD areas. Of note, one of the two IPMN with invasive PDAC had B-cell lymphoid aggregates.

Analysis of differentially expressed immune biomarkers using a validation set

On the basis of the results obtained in the training set, we interrogated a validation set of 93 IPMN samples. For this purpose, the mIF panel which revealed differential expression between LG-IPMN and HG-IPMN in the training set (CD3, CD8, PD1, CD68) was used. The clinicopathologic characteristics available from samples of this set are described in Supplementary Table S12. The mIF analysis showed that PD-L1 was not expressed in neoplastic cells of IPMN, irrespective of grade of dysplasia. Analogous to the findings of the training set, we observed that in the dysplastic epithelial compartment, total and cytotoxic T cells had higher densities in isolated LGD from LG-IPMNs, compared with progressor LGD from HG-IPMNs, and HGD of HG-IPMN. Moreover, in this set, analysis of the dysplastic epithelial compartment showed higher densities of antigen-experienced T cells and macrophages in isolated LGD from LG-IPMN compared

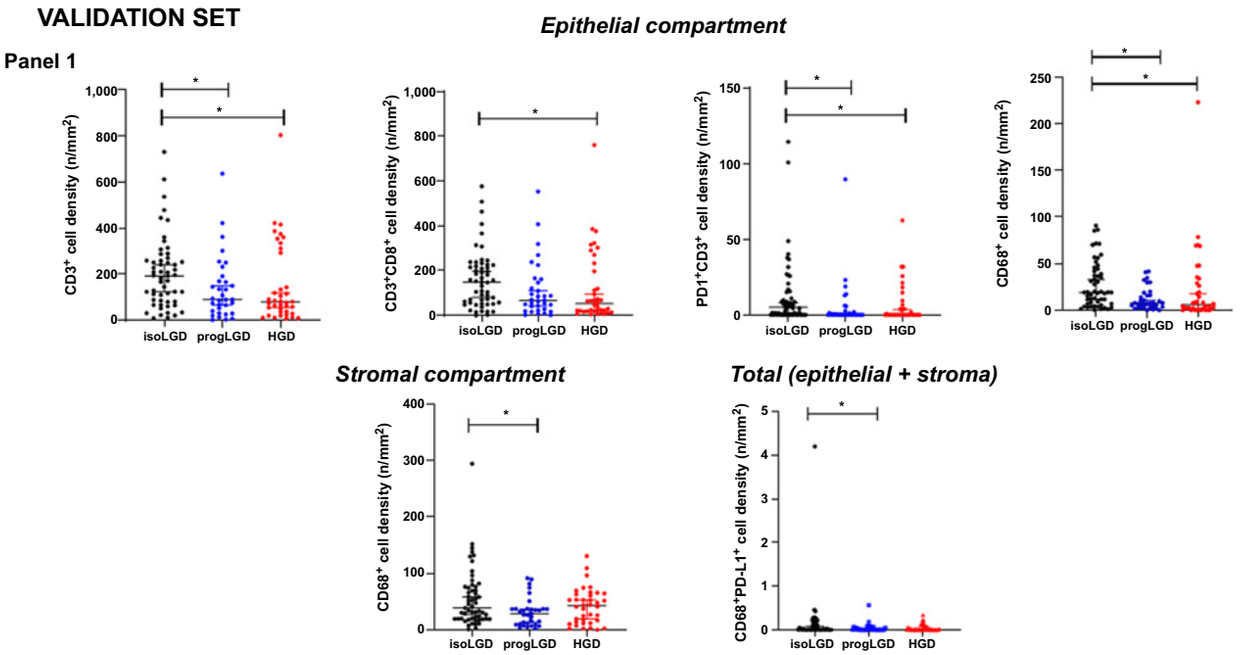

Figure 4.

Scatter dot plot showing differential distribution of immune cell densities in the different compartments of the Validation set, among dysplasia areas of low-grade IPMN and high-grade IPMN (isoLGD, isolated LGD area of low-grade IPMN; progLGD, progressive low-grade dysplasia area of high-grade IPMN; HGD, high-grade dysplasia area of high-grade IPMN). Dysplastic epithelial compartment panel 1: $CD3^+$, $CD3^+CD8^+$, $PD1^+CD3^+$, $CD68^+$; Stromal compartment panel 1: $CD68^+$; Total compartment panel 1: $CD68^+PD\text{-}L1^+$. Differences between all groups were determined using Kruskal–Wallis, and differences between two groups were determined by *t* test (ns, nonsignificant). Black bars indicate median and 95% confidence Interval.

with progressor LGD of HG-IPMNs, and the differences of macrophages were also evident when we analyzed dysplastic epithelial and stromal compartment together (**Fig. 4**).

Discussion

In this study, we profiled immune cell infiltration in the dysplastic epithelial/carcinoma and stromal compartments of IPMN, *bona fide* precursor lesions of PDAC, at different grades of dysplasia to assess the role of immune surveillance in progression of the disease. Although immune cell infiltration profiles across sample cohorts were heterogenous, HG-IPMN showed overall diminished immune response compared with LG-IPMN, most notably with significant reduction in total and cytotoxic T cells in HGD as well as in progressor LGD lesions of HG-IPMN. Our previous work had revealed that spatial proximities between epithelial cells of IPMNs and T cells may be predictive of degree of dysplasia (25). These results are in accordance with other findings from IHC and single-cell transcriptomics analyses of IPMN (6, 20), in which higher abundance of T cells, especially cytotoxic T cells, were detected in LG-IPMN compared with HG-IPMN and PDAC. Of note, the difference in T-cell infiltrates, observed in our study, was predominantly in the dysplastic epithelial compartment rather than in the distal stromal compartment, indicating that peritumoral immune response evolves toward an immunosuppressive state, possibly involving mechanisms of immune evasion activated early during progression of PDAC. One of the mechanisms involved in low T-cell infiltration may be attributed to defects in antigen presentation as previous studies have shown that in genetically engineered mice model (KPC) of pancreatic carcinogenesis, pancreatic intraepithelial neoplasia (PanIN) lesions have scarce infiltration of conventional type 1 dendritic cells which lead to defects in T-cell response (26, 27). In addition, different mechanisms of immune evasion associated with distinct genetic or epigenetic alterations in preneoplastic lesions may also lead to disparate immune response seen in PDAC subtypes identified on the basis of genetic and immunophenotypic classifications (14–17). Our current findings warrant further investigation, including correlations with genetic abnormalities in preneoplastic lesions. A recent IHC-based study has reported that pancreatic IPMN microenvironment evolves from an immune active state represented by diverse T-cell repertoire comprising of $CD8^+$T cells, and T-cell subsets Th/c1 and Th/c2 as major components to a Treg dominated immunosuppressive state during progression to invasive pancreatic cancer (20). Absence of a shift in $FOXP3^+$ Treg profiles between HG-IPMN and LG-IPMN in our study suggests that this transition may be less involved during progressive development of dysplasia and becomes a more prevalent mechanism of immune suppression during progression to invasive disease.

Analyses of total $CD68^+$ TAMs and those expressing PD-L1 (the ligand for programmed death 1 receptor), the immune checkpoint marker activated for immune evasion, revealed no significant differences in the HG- and LG-IPMN samples of the training set. However, in the validation set, densities of total TAMs and PD-L1–expressing TAMs were elevated in isolated LGD compared with progressor LGD and HGD areas of HG-IPMN with the differences being more pronounced for the total TAMs in the dysplastic epithelial compartment and PD-L1–expressing TAMs in the stromal compartment. TAMs

have been associated with immune-suppressive functions and worse prognosis in PDAC, with infiltration in the stroma of premalignant lesions contributing to progression of disease (28, 29). While our results demonstrate that $CD68^+$ TAMs infiltrate isolated LGD, as previously reported, their similar or lower recruitment in progressor LGD or HGD areas of HG-IPMN suggests that, rather than the extent of infiltration, possible changes in the polarization spectrum of TAMs may be functionally more critical for the development of the dysplastic state of IPMN lesions (30). In addition, previous observations by IHC and single-cell transcriptomics analyses (6, 20) that TAM and MDSCs are higher in PDAC compared with LG- and HG-IPMN warrant more in-depth profiling of myeloid cells to determine their role in the pathogenesis of PDAC as well as the role of myeloid axis as possible immunotherapy target (31). Validation of the concept would require mIF assay at single-cell level of coexpressing protein markers exclusive for TAM polarization in HG and LG lesions.

We also evaluated the role of B cells in IPMN and in concordance with other studies, observed that B-cell densities were relatively low (6, 32) in most cases. However, paired analysis between progressor LGD and HGD areas of HG-IPMN showed that $CD20^+$ cell densities were significantly higher in progressor LGD. B cells have dual roles in immunity, with antitumor and protumor function (33), and detailed profiling of B-cell subsets may help understand the state of these cells in IPMN (34), although scarce number of B cells in the premalignant lesions, in general, may pose a challenge in undertaking such analyses. We further tried to characterize the structural context of development and infiltration of B cells by examining the presence of B-cell lymphoid aggregates [as surrogate of tertiary lymphoid structures (TLS)] which are associated with B-cell activation. Published reports have described the presence of TLS within PDAC microenvironment as a favorable prognosticator of antitumor immune response (35, 36). We, therefore, tried to characterize the structural context of development and infiltration of B cells by examining the presence of B-cell lymphoid aggregates (as surrogate of TLS) which are associated with B-cell activation, but no significant associations was observed between LG-IPMN compared with HG-IPMN.

Interpretation of the findings being reported in the study requires consideration of some currently unavoidable technical constraints. Although our mIF panels included multiple markers associated with different immune cell types, we found limitations in the number of markers that can be multiplexed and lack of exclusive consensus markers for these cells which preclude more definitive conclusions at this time about the role of immune infiltrates in progressively dysplastic IPMN lesions. Further investigations using coexpressing markers specific for subset of myeloid, T, and B cells are warranted to fully characterize the immune landscape of these preneoplastic lesions. Furthermore, technical limitations of mIF assay along with tissue heterogeneity of these lesions did not allow the analysis of the whole lesion area, or stromal/epithelial compartmentalization of similar sizes within the ROI. Thus, our conclusions may be affected by enrichment and heterogenous spatial distribution of immunophenotypes in these compartments. To overcome this limitation, further studies interrogating spatial distribution and pairwise interactions of immune phenotypes (25) are warranted, which will provide a more illustrative overview of the immune landscape of these types of lesions. In our cohort, information on genetic abnormalities was not available, therefore association of genomic signatures with immune phenotypes could not be performed; in addition, the size of our cohort may still be considered relatively small, and the analysis of the degree of dysplasia may have observational bias without adjusting for multiple comparisons. In this regard, larger scale validation of these findings will require analyses with more informative marker panels of additional cases including IPMN with associated invasive adenocarcinoma.

In conclusion, we characterized the TIME of LG- and HG-IPMN using selected innate and adaptive immune markers employing mIF, IHC, and high-resolution image analysis approaches. Results revealed depletion of immune response during progression of LG- to HG-IPMN. Interestingly, however, immune phenotype of LG-IPMNs that had progressed at the time of surgical resection (progressor LGD lesions) resembled that of the synchronous HG-IPMNs, underscoring that attenuated immune surveillance occurs even in LG-IPMNs destined for progression. The finding, thus, indicates that effective clinical interception of cystic neoplasia to PDAC may be achievable through maintenance of sustained immune surveillance using vaccines and other prevention approaches. Recent advances in the development of endoscopic ultrasound–guided pancreatic cyst wall microbiopsy technique for improved diagnosis (37) of cystic neoplasms raise the possibility that clinical interception with maintenance of immune surveillance may indeed be achievable for these preinvasive neoplastic lesions.

Authors' Disclosures

C. Haymaker reports other support from Briacell, as well as personal fees from Nanobiotix outside the submitted work. M. Yip-Schneider reports grants from NIH during the conduct of the study, as well as grants from NIH outside the submitted work. M.A. Firpo reports grants from NIH during the conduct of the study; in addition, M.A. Firpo has a patent 10,451,628 issued. E.J. Koay reports grants from NIH, DOD, SU2C, Elekta, GE Healthcare, Philips Healthcare, and EMD Serono during the conduct of the study, as well as personal fees from RenovoRx, Taylor and Francis LLC, Apollo Health, MD Anderson Physicians Network, and AstraZeneca outside the submitted work. I.I. Wistuba reports grants and personal fees from Genentech/Roche, Bayer, Bristol Myers Squibb, AstraZeneca, Pfizer, HTG Molecular, Merck, Guardant Health, Novartis, Sanofi Aventis, and Amgen; personal fees from GlaxoSmithKline, Flame, Daiichi Sankyo, Janssen, Oncocyte, Medscape, Aptitute Health, OncLive, and Platform Health; and grants from Medimmune, 4D, Adaptimmune, Takeda, EMD Serono, Johnson & Johnson, Karus, Iovance, and Akoya outside the submitted work. A. Maitra reports grants from NIH/NCI and MD Anderson Cancer Center during the conduct of the study. A. Maitra also reports other support from Cosmos Wisdom Biotechnology and Thrive Earlier Detection (an Exact Sciences company), as well as personal fees from Freenome and Tezcat Biotech outside the submitted work. S. Sen reports grants from NCI/NIH during the conduct of the study. No disclosures were reported by the other authors.

Authors' Contributions

S. Hernandez: Data curation, formal analysis, supervision, investigation, methodology, writing–original draft, writing–review and editing. **E.R. Parra:** Conceptualization, formal analysis, supervision, investigation, writing–review and editing. **N. Uraoka:** Formal analysis, supervision, methodology. **X. Tang:** Formal analysis, investigation. **Y. Shen:** Data curation, formal analysis, methodology. **W. Qiao:** Data curation, formal analysis, methodology. **M. Jiang:** Investigation, methodology. **S. Zhang:** Data curation, methodology. **B. Mino:** Investigation, methodology. **W. Lu:** Investigation, methodology. **R. Pandurengan:** Data curation, methodology. **C. Haymaker:** Data curation, supervision, visualization, methodology, writing–review and editing. **K. Affolter:** Conceptualization, investigation. **C.L. Scaife:** Conceptualization, investigation. **M. Yip-Schneider:** Conceptualization, investigation. **C.M. Schmidt:** Conceptualization, investigation. **M.A. Firpo:** Conceptualization, investigation. **S.J. Mulvihill:** Conceptualization, investigation. **E.J. Koay:** Conceptualization, investigation. **H. Wang:** Conceptualization, investigation, methodology. **I.I. Wistuba:** Conceptualization, resources, formal analysis, supervision, investigation, methodology. **A. Maitra:** Conceptualization, resources, supervision, investigation, project administration, writing–review and editing. **L.M. Solis:** Conceptualization, resources, data curation, formal analysis, supervision, investigation, methodology, writing–original draft, writing–review and editing.

S. Sen: Conceptualization, resources, supervision, investigation, project administration, writing–review and editing.

Acknowledgments

A. Maitra and S. Sen are supported by U01 CA196403, U01 CA200468, UO1 CA 214263, P50 CA221707, and U24 CA224020. This project was also supported in part by The Translational Molecular Pathology Immunoprofiling Laboratory (TMP-IL) at the Department of Translational Molecular Pathology and the Moonshot Program in Pancreatic Cancer at the University of Texas MD Anderson Cancer Center (Houston, TX). We thank Dr. Arvind Rao and Dr. Souptik Barua for their help and comments for spatial analysis discussion, as well as Dr. Michael P. Kim, Dr. Matthew H.G. Katz and Dr. Mark Hurd for their help with sample accrual.

The costs of publication of this article were defrayed in part by the payment of page charges. This article must therefore be hereby marked *advertisement* in accordance with 18 U.S.C. Section 1734 solely to indicate this fact.

Received July 16, 2021; revised October 2, 2021; accepted February 21, 2022; published first February 23, 2022.

References

1. Tanaka M, Fernandez-Del Castillo C, Kamisawa T, Jang JY, Levy P, Ohtsuka T, et al. Revisions of international consensus Fukuoka guidelines for the management of IPMN of the pancreas. Pancreatology 2017;17:738–53.
2. Matthaei H, Schulick RD, Hruban RH, Maitra A. Cystic precursors to invasive pancreatic cancer. Nat Rev Gastroenterol Hepatol 2011;8:141–50.
3. Marchegiani G, Mino-Kenudson M, Sahora K, Morales-Oyarvide V, Thayer S, Ferrone C, et al. IPMN involving the main pancreatic duct: biology, epidemiology, and long-term outcomes following resection. Ann Surg 2015;261:976–83.
4. Hackert T, Fritz S, Klauss M, Bergmann F, Hinz U, Strobel O, et al. Main-duct intraductal papillary mucinous neoplasm: high cancer risk in duct diameter of 5 to 9 mm. Ann Surg 2015;262:875–80.
5. Basturk O, Hong SM, Wood LD, Adsay NV, Albores-Saavedra J, Biankin AV, et al. A revised classification system and recommendations from the Baltimore consensus meeting for neoplastic precursor lesions in the pancreas. Am J Surg Pathol 2015;39:1730–41.
6. Bernard V, Semaan A, Huang J, San Lucas FA, Mulu FC, Stephens BM, et al. Single-cell transcriptomics of pancreatic cancer precursors demonstrates epithelial and microenvironmental heterogeneity as an early event in neoplastic progression. Clin Cancer Res 2019;25:2194–205.
7. He J, Cameron JL, Ahuja N, Makary MA, Hirose K, Choti MA, et al. Is it necessary to follow patients after resection of a benign pancreatic intraductal papillary mucinous neoplasm? J Am Coll Surg 2013;216:657–65.
8. Payne SN, Maher ME, Tran NH, Van De Hey DR, Foley TM, Yueh AE, et al. PIK3CA mutations can initiate pancreatic tumorigenesis and are targetable with PI3K inhibitors. Oncogenesis 2015;4:e169.
9. Rooney SL, Shi J. Intraductal tubulopapillary neoplasm of the pancreas: an update from a pathologist's perspective. Arch Pathol Lab Med 2016;140:1068–73.
10. Omori Y, Ono Y, Tanino M, Karasaki H, Yamaguchi H, Furukawa T, et al. Pathways of progression from intraductal papillary mucinous neoplasm to pancreatic ductal adenocarcinoma based on molecular features. Gastroenterology 2019;156:647–61.
11. Kabacaoglu D, Ciecielski KJ, Ruess DA, Algul H. Immune checkpoint inhibition for pancreatic ductal adenocarcinoma: current limitations and future options. Front Immunol 2018;9:1878.
12. Bear AS, Vonderheide RH, O'Hara MH. Challenges and opportunities for pancreatic cancer immunotherapy. Cancer Cell 2020;38:788–802.
13. Ho WJ, Jaffee EM, Zheng L. The tumour microenvironment in pancreatic cancer - clinical challenges and opportunities. Nat Rev Clin Oncol 2020;17:527–40.
14. Moffitt RA, Marayati R, Flate EL, Volmar KE, Loeza SG, Hoadley KA, et al. Virtual microdissection identifies distinct tumor- and stroma-specific subtypes of pancreatic ductal adenocarcinoma. Nat Genet 2015;47:1168–78.
15. Wartenberg M, Cibin S, Zlobec I, Vassella E, Eppenberger-Castori S, Terracciano L, et al. Integrated genomic and immunophenotypic classification of pancreatic cancer reveals three distinct subtypes with prognostic/predictive significance. Clin Cancer Res 2018;24:4444–54.
16. Bailey P, Chang DK, Nones K, Johns AL, Patch AM, Gingras MC, et al. Genomic analyses identify molecular subtypes of pancreatic cancer. Nature 2016;531:47–52.
17. Collisson EA, Sadanandam A, Olson P, Gibb WJ, Truitt M, Gu S, et al. Subtypes of pancreatic ductal adenocarcinoma and their differing responses to therapy. Nat Med 2011;17:500–3.
18. Lupinacci RM, Goloudina A, Buhard O, Bachet JB, Marechal R, Demetter P, et al. Prevalence of microsatellite instability in intraductal papillary mucinous neoplasms of the pancreas. Gastroenterology 2018;154:1061–5.
19. Beatty PL, van der Geest R, Hashash JG, Kimura T, Gutkin D, Brand RE, et al. Immunobiology and immunosurveillance in patients with intraductal papillary mucinous neoplasms (IPMNs), premalignant precursors of pancreatic adenocarcinomas. Cancer Immunol Immunother 2016;65:771–8.
20. Roth S, Zamzow K, Gaida MM, Heikenwalder M, Tjaden C, Hinz U, et al. Evolution of the immune landscape during progression of pancreatic intraductal papillary mucinous neoplasms to invasive cancer. EBioMedicine 2020;54:102714.
21. Parra ER, Jiang M, Solis L, Mino B, Laberiano C, Hernandez S, et al. Procedural requirements and recommendations for multiplex immunofluorescence tyramide signal amplification assays to support translational oncology studies. Cancers 2020;12:255.
22. Parra ER, Uraoka N, Jiang M, Cook P, Gibbons D, Forget MA, et al. Validation of multiplex immunofluorescence panels using multispectral microscopy for immune-profiling of formalin-fixed and paraffin-embedded human tumor tissues. Sci Rep 2017;7:13380.
23. World Medical Association. World Medical Association Declaration of Helsinki: ethical principles for medical research involving human subjects. JAMA 2013;310:2191–4.
24. Bergomas F, Grizzi F, Doni A, Pesce S, Laghi L, Allavena P, et al. Tertiary intratumor lymphoid tissue in colo-rectal cancer. Cancers 2011;4:1–10.
25. Barua S, Solis L, Parra ER, Uraoka N, Jiang M, Wang H, et al. A functional spatial analysis platform for discovery of immunological interactions predictive of low-grade to high-grade transition of pancreatic intraductal papillary mucinous neoplasms. Cancer Inform 2018;17:1176935118782880.
26. Hegde S, Krisnawan VE, Herzog BH, Zuo C, Breden MA, Knolhoff BL, et al. Dendritic cell paucity leads to dysfunctional immune surveillance in pancreatic cancer. Cancer Cell 2020;37:289–307.
27. Lin JH, Huffman AP, Wattenberg MM, Walter DM, Carpenter EL, Feldser DM, et al. Type 1 conventional dendritic cells are systemically dysregulated early in pancreatic carcinogenesis. J Exp Med 2020;217:e20190673.
28. Di Caro G, Cortese N, Castino GF, Grizzi F, Gavazzi F, Ridolfi C, et al. Dual prognostic significance of tumour-associated macrophages in human pancreatic adenocarcinoma treated or untreated with chemotherapy. Gut 2016;65:1710–20.
29. Murray PJ. Macrophage polarization. Annu Rev Physiol 2017;79:541–66.
30. Knudsen ES, Vail P, Balaji U, Ngo H, Botros IW, Makarov V, et al. Stratification of pancreatic ductal adenocarcinoma: combinatorial genetic, stromal, and immunologic markers. Clin Cancer Res 2017;23:4429–40.
31. Candido JB, Morton JP, Bailey P, Campbell AD, Karim SA, Jamieson T, et al. CSF1R(+) macrophages sustain pancreatic tumor growth through T cell suppression and maintenance of key gene programs that define the squamous subtype. Cell Rep 2018;23:1448–60.
32. Hernandez-Barco YG, Bardeesy N, Ting DT. No cell left unturned: intraductal papillary mucinous neoplasm heterogeneity. Clin Cancer Res 2019;25:2027–9.
33. Gunderson AJ, Kaneda MM, Tsujikawa T, Nguyen AV, Affara NI, Ruffell B, et al. Bruton tyrosine kinase-dependent immune cell cross-talk drives pancreas cancer. Cancer Discov 2016;6:270–85.

34. Schwartz M, Zhang Y, Rosenblatt JD. B cell regulation of the anti-tumor response and role in carcinogenesis. J Immunother Cancer 2016; 4:40.
35. Hiraoka N, Ino Y, Yamazaki-Itoh R, Kanai Y, Kosuge T, Shimada K. Intratumoral tertiary lymphoid organ is a favourable prognosticator in patients with pancreatic cancer. Br J Cancer 2015;112:1782–90.
36. Stromnes IM, Hulbert A, Pierce RH, Greenberg PD, Hingorani SR. T-cell localization, activation, and clonal expansion in human pancreatic ductal adenocarcinoma. Cancer Immunol Res 2017;5:978–91.
37. Vestrup Rift C, Melchior LC, Kovacevic B, Toxvaerd A, Klausen P, Karstensen JG, et al. Next-generation sequencing of endoscopic ultrasound guided microbiopsies from pancreatic cystic neoplasms. Histopathology 2019;75:767–71.